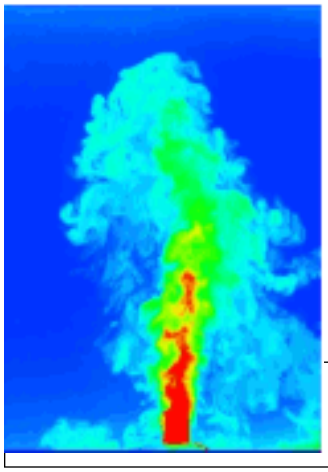

Journal of Turbulence
Publication details, including instructions for authors and subscription information:
http://www.informaworld.com/smpp/title~content=t713665472

# Investigation using statistical closure theory of the influence of the filter shape on scale separation in large-eddy simulation

J. Berland [a]; C. Bogey [a]; C. Bailly [a]
[a] Laboratoire de Mécanique des Fluides et d'Acoustique, Ecully, France

First Published on: 04 July 2008

To cite this Article: Berland, J., Bogey, C. and Bailly, C. (2008) 'Investigation using statistical closure theory of the influence of the filter shape on scale separation in large-eddy simulation', Journal of Turbulence, Volume 9, Art. No. N21,

To link to this article: DOI: 10.1080/14685240802244116
URL: http://dx.doi.org/10.1080/14685240802244116

*Journal of Turbulence*
Vol. 9, No. 21, 2008, 1–22





# Investigation using statistical closure theory of the influence of the filter shape on scale separation in large-eddy simulation

J. Berland*, C. Bogey and C. Bailly

*Laboratoire de Mécanique des Fluides et d'Acoustique, UMR CNRS 5509, Ecole Centrale de Lyon, 69134 Ecully, France*

(*Received 9 October 2007; final version received 5 March 2008*)

The influence of the filter shape on scale separation in large-eddy simulation (LES) is investigated using the eddy-damped quasi-normal Markovian (EDQNM) modelling approach, for discrete filters of order 2–12. The LES subgrid-scale (SGS) stress tensor is split into a represented SGS tensor based on the scales resolved by the mesh, and a non-represented SGS tensor involving the unresolved scales. The investigation of the kinetic energy spectra associated with these quantities shows that the features of the SGS tensor strongly depend on the filter shape. In particular, for the second-order filter, the SGS stress tensor dynamics is dominated by the interactions between the resolved scales. The effective LES cut-off wavenumber is finally evaluated and recast in term of efficiency rates in order to estimate the computational cost required to achieve a given spectral resolution. Sharp cut-off filters appear to be well appropriate to perform an efficient scale separation in LES.

**Keywords:** large-eddy simulation; scale separation; filter shape; EDQNM

## 1. Introduction

Large-eddy simulations (LES) aim at reducing computational cost of flow calculations by separating the turbulence spectrum into small and large scales; the effects of the small ones being taken into account through a subgrid-scale model. Such calculations rely on the filtered Navier–Stokes equations which are obtained by applying a low-pass filter for the length scales to the Navier–Stokes equations, and are based on the hypothesis that larger scales are flow-dependent whereas the smaller ones possess a universal behaviour allowing physical modelling valid for a large variety of turbulent configurations [1].

Scale separation in LES is however a debatable issue since the theoretical framework of the filtered Navier–Stokes imposes few constraints on the filter [2], whose shape can be freely chosen. To achieve scale separation, the use of spectral filters seems appropriate since these filters act as projectors dividing scales in a clear manner. Nevertheless, due to the difficulty to design spectral operators in complex configurations, the practical implementation of LES commonly makes use of filters of various shapes such as the top-hat filter or some discrete filters with other formal order [3, 4]. The transition between completely removed scales and un-removed ones is then progressive and this transition in the filter transfer function makes classification into small/large, filtered/unfiltered or resolved/unresolved scales more tedious.

*Corresponding author. Email: julien.berland@paris.ensam.fr

ISSN: 1468-5248 online only

DOI: 10.1080/14685240802244116
http://www.tandf.co.uk/journals

Scale classification can be clarified by introducing the notational convention of Domaradzki and Adams [5] who explicitly make reference to the spectral filtering performed by the mesh into the filtered Navier–Stokes equations. This formalism allows us in particular to demonstrate that the subgrid-scale (SGS) tensor can be decomposed into two contributions, one representing interactions between scales resolved by the mesh and another taking into account the couplings involving unresolved scales. It is hence relevant to determine for a given filter shape to what extent the SGS stress tensor truly represents interactions between scales lying in the inertial range and displaying a universal behaviour. When it is not the case, the universality assumption allowing the design of robust SGS models is not fulfilled. Scale separation into small and large ones is not achieved and SGS modelling becomes similar to RANS (Reynolds-average Navier–Stokes) techniques since the large scales need to be modelled [6]. The problematic of scale separation also encompasses the issue of the definition of the wavenumber cut-off of the LES which may have an influence on the computed statistics [7]. The grid size defines an upper limit for the resolved wavenumbers, but introducing non-spectral filters into the filtered Navier–Stokes equations may shift the effective wavenumber cut-off towards larger scales. Using low-dissipation filters, a wavenumber cut-off at about four grid points per scale can be for instance obtained [8].

Qualitative discussions of the interplay between the SGS energy transfers, the filter shape and the grid have been proposed for instance by Carati et al. [9], Langford and Moser [10] or Domaradzki and Loh [11,12]. Piomelli, Moin, and Ferziger [13] carried out numerical experiments on LES of turbulent channel flows. They demonstrate that the LES filter has a strong influence on SGS modelling since accurate results were obtained only with some LES filter/SGS model combinations. Leslie and Quarini [14] moreover showed using theoretical developments that the magnitude of the subgrid and Leonard stress tensors strongly depends on the filter shape. Yang and Fu [15] also studied the effect of the filtering on the resolution of the truncated Navier–Stokes equations and established that the filter type has a direct influence on simulation results. High-order filters turned out to exhibit accurate results for their calculations. De Stefano and Vasilyev [6] finally have investigated the influence of the filter shape on subgrid modelling for the one-dimensional Burger's equation. Their works show that for smooth filters the SGS stress tensor can have contribution from the large scales, whereas for sharp cut-off filters the SGS stress tensor mainly represents small-scale dynamics.

The present work focuses on the study of the influence of the filter transfer function on scale separation in LES of homogeneous isotropic freely decaying turbulence. In particular, contributions from resolved and unresolved scales to the SGS stress tensor are quantified in details for discrete filters of various orders and for optimized filters [3]. Following Domaradzki and Adams [5] the SGS stress tensor is divided into two parts corresponding respectively to the interactions between resolved scales and to the interactions involving non-resolved scales. These two components are evaluated using the eddy-damped quasi-normal Markovian (EDQNM) approximation for a Reynolds number $Re_\lambda = 2500$ based on the transversal Taylor scale. Post-processing of direct numerical simulation (DNS) data could be performed with the same aim in view as for instance in Domaradzki and Carati [16]. However, even though stochastic closure models have some limitations due to their underlying assumptions, they can nevertheless easily provide detailed information on flow physics at high Reynolds numbers while maintaining computational cost at a reasonable level. The technique was formerly used for instance by Schilling and Zhou [17]. The contributions from each scale to the SGS stress tensor are thus determined using an EDQNM approach in order to assess for a given filter whether large-scale dynamics plays a role into SGS modelling and hence whether scale separation is properly performed. The effective LES cut-off wavenumber is finally determined by the evaluation of scale contributions to the SGS stress tensor. It must be emphasized that the present investigation does not tackle with SGS modelling itself, but rather with the interpretation of the SGS stress tensor for different filter shapes.

In this paper, the filtered Navier–Stokes and the corresponding EDQNM modelling are described in Section 2. Results of the EDQNM calculation for a Reynolds number $Re_\lambda = 2500$, scale separation and LES effective cut-off are then discussed in Section 3 for several discrete filters. Concluding remarks are finally drawn in Section 4.

## 2. Governing equations

### 2.1. *Filtered Navier–Stokes equations*

#### 2.1.1. *Physical space*

Scale separation in LES and derivation of the filtered Navier–Stokes equations traditionally rely on the application of an explicit filtering to the governing equations. In an attempt to define a framework for the deconvolution approach, Domaradzki and Adams [5] proposed to introduce an additional projection operator. The projection of a flow solution on a grid indeed leads implicitly to a spectral filtering of the flow variables at the cut-off wavenumber $k_c = \pi/\Delta$, where $\Delta$ is the mesh size. Notations indicating explicitly the spatial filtering as well as the spectral projection can therefore be used to better understand the influence of the filter shape on further physical modelling.

Following the works of Domaradzki and Adams [5], flow variables are decomposed into two contributions

$$f = f^{\mathcal{L}} + f^{\mathcal{S}}, \tag{1}$$

where the spectral truncation at the mesh cut-off wavenumber $k_c$ is denoted by the upperscript $\mathcal{L}$ and its complement by $\mathcal{S}$. Spatial filtering is indicated by the common overbar notation. This theoretical framework gives the opportunity to define some terminology which will be used in the remainder of this paper. Consider for instance a field $f$. The following definitions are introduced: $f$ is the unfiltered field, $f^{\mathcal{L}}$ is the resolved field and $f^{\mathcal{S}}$ is the unresolved field. The filtered field is given by $\overline{f^{\mathcal{L}}} = \overline{f}^{\mathcal{L}} = \overline{f}$, the equalities holding true as long as the support of the transfer function of the filter remains within the spectral resolution of the mesh.

Assuming that spectral truncation and spatial filtering commute, the filtered Navier–Stokes equations can be written as

$$\frac{\partial \overline{u}_i^{\mathcal{L}}}{\partial t} + \frac{\partial}{\partial x_j}\left(\overline{u_i u_j}^{\mathcal{L}}\right) - \frac{1}{\rho}\frac{\partial \overline{p}^{\mathcal{L}}}{\partial x_i} - \nu \frac{\partial^2 \overline{u}_i^{\mathcal{L}}}{\partial x_j^2} = 0. \tag{2}$$

The nonlinear product $u_i u_j$ is then decomposed as

$$\overline{u_i u_j}^{\mathcal{L}} = \left(\overline{u}_i^{\mathcal{L}} \overline{u}_j^{\mathcal{L}}\right)^{\mathcal{L}} + \left[\overline{u_i^{\mathcal{L}} u_j^{\mathcal{L}}}^{\mathcal{L}} - \left(\overline{u}_i^{\mathcal{L}} \overline{u}_j^{\mathcal{L}}\right)^{\mathcal{L}}\right] + \overline{u_i^{\mathcal{L}} u_j^{\mathcal{S}} + u_i^{\mathcal{S}} u_j^{\mathcal{L}} + u_i^{\mathcal{S}} u_j^{\mathcal{S}}}^{\mathcal{L}}, \tag{3}$$

so that the subgrid-scale stress tensor includes two terms

$$\tau_{ij}^{\mathrm{rep}} = \overline{u_i^{\mathcal{L}} u_j^{\mathcal{L}}}^{\mathcal{L}} - \left(\overline{u}_i^{\mathcal{L}} \overline{u}_j^{\mathcal{L}}\right)^{\mathcal{L}}, \tag{4}$$

$$\tau_{ij}^{\mathrm{nrp}} = \overline{u_i^{\mathcal{L}} u_j^{\mathcal{S}} + u_i^{\mathcal{S}} u_j^{\mathcal{L}} + u_i^{\mathcal{S}} u_j^{\mathcal{S}}}^{\mathcal{L}}. \tag{5}$$

The tensor $\tau_{ij}^{\mathrm{rep}}$ represents the nonlinear interactions within scales present on the grid whereas $\tau_{ij}^{\mathrm{nrp}}$ takes into account interactions involving non-resolved scales [5].

### 2.1.2. *Spectral space*

Let us now consider the above developments in the spectral space. The Navier–Stokes equations for an incompressible flow reads in the Fourier space [18]

$$\left(\frac{\partial}{\partial t} + \nu k^2\right)\widehat{u}_i(\mathbf{k}) = M_{imn}(\mathbf{k}) \iint \widehat{u}_m(\mathbf{p})\widehat{u}_n(\mathbf{q})\delta_{\mathbf{k}-\mathbf{p}-\mathbf{q}}\,\mathrm{d}\mathbf{p}\mathrm{d}\mathbf{q}, \tag{6}$$

where the integral is performed over $\mathbb{R}^3 \times \mathbb{R}^3$ and $\widehat{u}_i(\mathbf{k})$ is the Fourier coefficient of the velocity component $u_i$ for the wavenumber vector $\mathbf{k} = (k_i)$. The projection operators are defined by the relationships

$$M_{imn}(\mathbf{k}) = -\mathrm{i}P_{imn}(\mathbf{k}), \tag{7}$$

$$P_{imn}(\mathbf{k}) = (k_n P_{im} + k_m P_{in})/2, \tag{8}$$

$$P_{ij} = \delta_{ij} - k_i k_j / k^2. \tag{9}$$

Assuming that the operators are isotropic, spatial filtering and spectral truncation are respectively equivalent in the spectral space to a multiplication of the Fourier coefficients by the quantities $G_k$ and $P_k$, where $G_k$ is the Fourier transform of the filter kernel and $P_k$ is equal to 1 for $k \leq k_c$ and zero otherwise. The filter support is furthermore assumed to remain within the grid spectral resolution, i.e. $G_k = 0$ for $k > k_c$, and $P_k G_k = G_k$ for any wavenumber $k$.

Applying $G_k$ and $P_k$ to Equation (6) yields the filtered incompressible Navier–Stokes equations in the spectral space

$$\left(\frac{\partial}{\partial t} + \nu k^2\right)[P_k G_k \widehat{u}_i(\mathbf{k})] = P_k G_k M_{imn}(\mathbf{k}) \iint \widehat{u}_m(\mathbf{p})\widehat{u}_n(\mathbf{q})\delta_{\mathbf{k}-\mathbf{p}-\mathbf{q}}\,\mathrm{d}\mathbf{p}\mathrm{d}\mathbf{q}, \tag{10}$$

where $P_k G_k \widehat{u}_i(\mathbf{k}) = \widehat{\overline{u}_i^{\mathcal{L}}}(\mathbf{k}) = \widehat{\overline{u}_i}(\mathbf{k})$ corresponds to the filtered velocity field. The right-hand side, which contains all the triadic interactions $(\mathbf{k}, \mathbf{p}, \mathbf{q})$, such as $\mathbf{k} = \mathbf{p} + \mathbf{q}$, can be rewritten by introducing a decomposition similar to that proposed in Equation (3) in the physical space. One may indeed write that

$$\begin{aligned} P_k G_k = {} & \overbrace{P_p G_p P_q G_q P_k}^{\gamma_{kpq}^{\mathrm{nl}}} + \overbrace{\left(P_p P_q G_k P_k - P_p G_p P_q G_q P_k\right)}^{\gamma_{kpq}^{\mathrm{rep}}} \\ & + \underbrace{\left[P_p(1-P_q) + (1-P_p)P_q + (1-P_p)(1-P_q)\right] G_k P_k}_{\gamma_{kpq}^{\mathrm{nrp}}}. \end{aligned} \tag{11}$$

The derivation of Equation (11) is similar to the analysis of Leslie and Quarini [14] and is deduced from the SGS stress tensor formulation (3) of Domaradzki and Adams [5] using the following algebra: $\widehat{\overline{f}}(\mathbf{k}) = G_k \widehat{f}(\mathbf{k})$, $\widehat{f^{\mathcal{L}}}(\mathbf{k}) = P_k \widehat{f}(\mathbf{k})$ and $\widehat{f^{\mathcal{S}}}(\mathbf{k}) = (1 - P_k)\widehat{f}(\mathbf{k})$. Equation (10) for the

filtered velocity hence read as

$$\left(\frac{\partial}{\partial t}+\nu k^2\right)[P_k G_k \widehat{u}_i(\mathbf{k})] = M_{imn}(\mathbf{k}) \iint \left(\gamma^{\mathrm{nl}}_{kpq}+\gamma^{\mathrm{rep}}_{kpq}+\gamma^{\mathrm{nrp}}_{kpq}\right)\widehat{u}_m(\mathbf{p})\widehat{u}_n(\mathbf{q})\delta_{\mathbf{k}-\mathbf{p}-\mathbf{q}}\,\mathrm{d}\mathbf{p}\mathrm{d}\mathbf{q}. \tag{12}$$

Finally, using the assumption that the filter support is restricted to the grid resolution ($P_k G_k = G_k$ for any $k$), Equation (12) is recast into

$$\left(\frac{\partial}{\partial t}+\nu k^2\right)[G_k \widehat{u}_i(\mathbf{k})] = M_{imn}(\mathbf{k}) \iint \left(\gamma^{\mathrm{nl}}_{kpq}+\gamma^{\mathrm{rep}}_{kpq}+\gamma^{\mathrm{nrp}}_{kpq}\right)\widehat{u}_m(\mathbf{p})\widehat{u}_n(\mathbf{q})\delta_{\mathbf{k}-\mathbf{p}-\mathbf{q}}\,\mathrm{d}\mathbf{p}\mathrm{d}\mathbf{q}, \tag{13}$$

with

$$\gamma^{\mathrm{nl}}_{kpq} = G_p G_q P_k, \tag{14}$$

$$\gamma^{\mathrm{rep}}_{kpq} = P_p P_q G_k - G_p G_q P_k, \tag{15}$$

$$\gamma^{\mathrm{nrp}}_{kpq} = [P_p(1-P_q)+(1-P_p)P_q+(1-P_p)(1-P_q)]G_k. \tag{16}$$

As in the physical space, the triadic interactions are now divided into three families. The couplings related to $\gamma^{\mathrm{nl}}_{kpq}$ represent the interactions between the filtered scales $\overline{u}_i$, whereas $\gamma^{\mathrm{nrp}}_{kpq}$ corresponds to interactions involving the unresolved scales $u_i^{\mathcal{S}}$. Due to the non-spectral filter shape one has also to take into account the interactions between the filtered field $\overline{u}_i$ and the resolved field $u_i^{\mathcal{L}}$. This is done by the term in Equation (12) involving $\gamma^{\mathrm{rep}}_{kpq}$.

The kinetic energy spectrum of the filtered velocity field is finally defined by $\overline{E}(k) = 2\pi k^2 G_k^2 \langle \widehat{u}_i(\mathbf{k})\widehat{u}_i(-\mathbf{k})\rangle$ where the brackets denote an ensemble average. The governing equation for the kinetic energy spectrum is thus obtained by multiplying (12) by $2\pi k^2 G_k \widehat{u}_i(-\mathbf{k})$, summing and averaging,

$$\left(\frac{\partial}{\partial t}+2\nu k^2\right)\overline{E}(k) = 4\pi k^2 G_k M_{imn}(\mathbf{k}) \iint \left(\gamma^{\mathrm{nl}}_{kpq}+\gamma^{\mathrm{rep}}_{kpq}+\gamma^{\mathrm{nrp}}_{kpq}\right) \times \langle \widehat{u}_m(\mathbf{p})\widehat{u}_n(\mathbf{q})\widehat{u}_i(-\mathbf{k})\rangle \delta_{\mathbf{k}-\mathbf{p}-\mathbf{q}}\,\mathrm{d}\mathbf{p}\mathrm{d}\mathbf{q}. \tag{17}$$

The triple velocity correlations into the integral now need to be closed to allow further developments.

### 2.2. *EDQNM closure*

#### 2.2.1. *Model derivation*

The closure of the triple velocity correlations in Equation (17) is carried out using the EDQNM approach, which is straightforward since the present theoretical developments are identical to those of the classical EDQNM theory. The coefficients $\gamma_{kpq}$ are indeed isotropic operators which can be easily introduced into the modelling process. The derivation of the model is not described here but further details may be found in the textbook of Lesieur [18] for instance, and a brief overview of the EDQNM technique is provided in Appendix. The time evolution of the kinetic

energy spectrum is then given by

$$\left(\frac{\partial}{\partial t} + 2\nu k^2\right)\overline{E}(k) = T^{\mathrm{nl}}(k) + T^{\mathrm{rep}}(k) + T^{\mathrm{nrp}}(k), \tag{18}$$

where time dependency of the variables is omitted for the sake of simplicity. The nonlinear energy transfers on the right-hand side are related to the $\gamma_{kpq}$ coefficients by

$$T^{\mathrm{nl}}(k) = G_k \iint_{\Delta_k} \gamma^{\mathrm{nl}}_{kpq} S(k, p, q)\,\mathrm{d}p\mathrm{d}q, \tag{19}$$

$$T^{\mathrm{rep}}(k) = G_k \iint_{\Delta_k} \gamma^{\mathrm{rep}}_{kpq} S(k, p, q)\,\mathrm{d}p\mathrm{d}q, \tag{20}$$

$$T^{\mathrm{nrp}}(k) = G_k \iint_{\Delta_k} \gamma^{\mathrm{nrp}}_{kpq} S(k, p, q)\,\mathrm{d}p\mathrm{d}q. \tag{21}$$

The integrand $S(k, p, q)$ is given by [18]

$$S(k, p, q) = \Theta_{kpq}(t)\frac{E(q)}{q}(xy + z^3)(k^2E(p) - p^2E(k)), \tag{22}$$

where $E(k) = 2\pi k^2\langle\widehat{u}_i(\mathbf{k})\widehat{u}_i(-\mathbf{k})\rangle$ is the kinetic energy spectrum of the unfiltered velocity field $u_i$. The geometrical coefficients $x$, $y$ and $z$, corresponding to the cosines of the interior angles of the triangle $(\mathbf{k}, \mathbf{p}, \mathbf{q})$, are given by

$$x = -\frac{p_i q_i}{pq}, \qquad y = -\frac{k_i q_i}{kq}, \qquad z = -\frac{p_i k_i}{pk}. \tag{23}$$

The integrations in Equations (19)–(21) are performed on the domain $\Delta_k$ defined by

$$\Delta_k = \{(p, q) \mid k + q \geq p \geq |k - q|\} = \{(p, q) \mid |z| \leq 1\}. \tag{24}$$

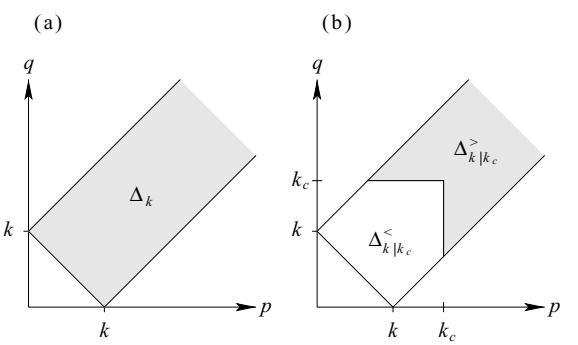


Figure 1. Sketch in the $(p, q)$-plane of the integration domains used to compute the nonlinear transfers for the EDQNM calculations. (a) Full domain and (b) separation into a resolved and a non-resolved domain given a cut-off wavenumber $k_c$.

A sketch of this set is given in Figure 1(a). The triple correlation relaxation time deduced from the EDQNM assumptions is provided by

$$\Theta_{kpq}(t) = \frac{1 - \exp[-\mu_{kpq}t - \nu(k^2 + p^2 + q^2)t]}{\mu_{kpq} + \nu(k^2 + p^2 + q^2)}, \tag{25}$$

with $\mu_{kpq} = \mu_k + \mu_p + \mu_q$. Modelling of the eddy damping rate $\mu_k$ is carried out by the formulation proposed by Lesieur [18]

$$\mu_k = 0.19 C_\eta^{3/2} \left[ \int_0^k k'^2 E(k') \, \mathrm{d}k' \right]^{1/2} \tag{26}$$

with a Kolmogorov constant [19] equal to 1.4.

As already pointed for the filtered velocity in Equation (12) in spectral space, gain and loss of energy at a wavenumber $k$ are due to three kinds of triadic interactions. The quantity $T^{\mathrm{nl}}(k)$ is referred to as the filtered nonlinear transfers and takes into account the interactions between filtered scales $\overline{u}_i$. The represented SGS nonlinear transfers $T^{\mathrm{rep}}(k)$ represent the couplings between the filtered field and the resolved field $u_i^{\mathcal{L}}$ and the non-represented SGS nonlinear transfers $T^{\mathrm{nrp}}(k)$ involve the unresolved field $u_i^{\mathcal{S}}$. While performing a LES, the filtered nonlinear transfers can be computed based only from knowledge of the filtered velocity. Determining the two other SGS quantities $T^{\mathrm{rep}}(k)$ and $T^{\mathrm{nrp}}(k)$ requires however knowledge of both the resolved and the unresolved fields $u_i^{\mathcal{L}}$ and $u_i^{\mathcal{S}}$. One can furthermore note that the sum of the represented SGS and non-represented SGS transfers corresponds to the classical subgrid-scale transfers, which are based on the definition $\tau_{ij} = \overline{u_i u_j} - \overline{u}_i \, \overline{u}_j$.

The explicit formulations (19)–(21) can be directly used to evaluate the nonlinear energy transfers $T^{\mathrm{nl}}(k)$, $T^{\mathrm{rep}}(k)$ and $T^{\mathrm{nrp}}(k)$. However, according to the limited support of the filter and of the spectral truncation, these energy transfers can be simplified. Consider first the resolved nonlinear transfers $T^{\mathrm{nl}}(k)$ given by

$$T^{\mathrm{nl}}(k) = G_k \iint_{\Delta_k} G_p G_q P_k S(k, p, q) \, \mathrm{d}p \mathrm{d}q. \tag{27}$$

Since the filter transfer function $G_k$ and the grid spectral truncation $P_k$ equal to zero for $k > k_c$, the integration domain can be reduced to the surface $\Delta^<_{k|k_c}$ defined by

$$\Delta^<_{k|k_c} = \{(p, q) \in \Delta_k \mid p \leq k_c \quad \text{and} \quad q \leq k_c\}. \tag{28}$$

A schematic view of this domain is presented in Figure 1(b). On this domain, $P_p$ and $P_q$ are furthermore equal to 1. The same remarks hold for the represented nonlinear energy transfers $T^{\mathrm{rep}}(k)$. Concerning the subgrid contribution $T^{\mathrm{nrp}}(k)$ of the non-resolved scales, one can note that the quantity

$$[P_p(1 - P_q) + (1 - P_p)P_q + (1 - P_p)(1 - P_q)], \tag{29}$$

equals 1 on the surface $\Delta^>_{k|k_c}$ defined by

$$\Delta^>_{k|k_c} = \{(p, q) \in \Delta_k \mid p > k_c \ \text{ or } q > k_c\}, \tag{30}$$

and is null elsewhere. The nonlinear energy transfers are finally given by

$$T^{\mathrm{nl}}(k) = G_k \iint_{\Delta^<_{k|k_c}} G_p G_q S(k,\, p,\, q)\, \mathrm{d}p\mathrm{d}q, \tag{31}$$

$$T^{\mathrm{rep}}(k) = G_k \iint_{\Delta^<_{k|k_c}} (G_k - G_p G_q) S(k,\, p,\, q)\, \mathrm{d}p\mathrm{d}q, \tag{32}$$

$$T^{\mathrm{nrp}}(k) = G_k^2 \iint_{\Delta^>_{k|k_c}} S(k,\, p,\, q)\, \mathrm{d}p\mathrm{d}q. \tag{33}$$

The nonlinear energy transfers $T^{\mathrm{SGS}}(k)$ associated with the classical SGS stress tensor is furthermore introduced as

$$T^{\mathrm{SGS}}(k) = G_k \iint_{\Delta_k} (G_k - G_p G_q) S(k,\, p,\, q)\, \mathrm{d}p\mathrm{d}q \tag{34}$$

and is such as $T^{\mathrm{rep}}(k) + T^{\mathrm{nrp}}(k) = T^{\mathrm{SGS}}(k)$.

Finally, some results will be interpreted in terms of the normalized spectral eddy viscosity [19] defined for any energy transfers $T(k)$ by

$$\nu_t^+(k/k_c) = \frac{T(k)}{-2k^2 E(k)} \sqrt{\frac{k_c}{E(k_c)}}. \tag{35}$$

The quantity $\nu_t^+(k/k_c)$ is an effective eddy viscosity acting on modes of wavenumber $k$. The investigation of the evolution of $\nu_t^+(k/k_c)$ with $k$ can provide details on the physics underlying the energy transfers [25].

### 2.2.2. *Detailed scale contribution to nonlinear energy transfers*

Given a nonlinear energy transfer $T(k)$ of the form

$$T(k) = \iint_{\Delta_k} \gamma_{kpq} S(k,\, p,\, q)\, \mathrm{d}p\mathrm{d}q, \tag{36}$$

it is interesting to determine which scales have a major contribution to the energy exchanges. Such a quantification can be performed using the following procedure. While computing an energy transfer, one can reduce the domain of integration and take into account only interactions between scales with wavenumbers $p$ and $q$ in (36) smaller than a given wavenumber $k'$. The surface of integration is hence reduced to $\Delta^<_{k|k'}$ which is defined by Equation (28). The integration on $\Delta^<_{k|k'}$ removes the contribution from the couplings between 'small' scales which are in this context scales with wavenumbers larger than $k'$. The results of the integration is denoted $T^<(k, k')$:

$$T^<(k, k') = \iint_{\Delta^<_{k|k'}} \gamma_{kpq} S(k,\, p,\, q)\, \mathrm{d}p\mathrm{d}q. \tag{37}$$

The differentiation with respect to $k'$ is denoted by $\zeta(k, k')$ and is defined by

$$\zeta(k, k') = \frac{\partial}{\partial k'}[T^{<}(k, k')]. \tag{38}$$

The quantity $\zeta(k, k')\,\mathrm{d}k'$ represents the net effect on the nonlinear energy transfer $T(k)$ when scales with wavenumbers between $k'$ and $k' + \mathrm{d}k'$ are taken into account.

The investigation of the evolution of $\zeta(k, k')$ for a given wavenumber $k$ as the cut-off $k'$ is varied permits to estimate which scales mostly contribute to the nonlinear energy transfer at a wavenumber $k$. It is referred to as the detailed scale contribution.

### 2.2.3. *Numerical resolution of the EDQNM model*

The numerical resolution of the integro-differential system (18) is achieved using a logarithmic wavenumber mesh given by

$$k_i = k_{\min} 2^{(i-1)/F}, \text{ for } i = 1, \ldots, N, \tag{39}$$

where $k_{\min}$ is the minimum wavenumber of the mesh, $F$ is the number of points per decade and $N$ is the total number of points. The algorithm of Leith [20] is used to evaluate the integrals defining the nonlinear transfers. The corrective term of Lesieur [18] is furthermore implemented to take into account non-local triadic couplings which are poorly resolved by Leith's scheme. Time stepping is performed using the Euler method and the time step is given by the relationship $\Delta t < 1/(\nu k_N^2)$.

The initial spectrum is provided by [17]

$$E(k) = 16\sqrt{\frac{2}{\pi}}\frac{v_0^2}{k_0}\left(\frac{k}{k_0}\right)^4 \exp\left[-2\left(\frac{k}{k_0}\right)^2\right]. \tag{40}$$

The wavenumber $k_0$ corresponds to the maximum of energy and $v_0$ is a typical velocity.

The Reynolds number is evaluated using the Taylor scale $\lambda$ as $Re_\lambda = \lambda v_0/\nu$ so that the viscosity $\nu$ is set in order to obtain a given Reynolds number. The non-dimensional time is denoted by $t^*$ and is given by $t^* = k_0 v_0 t$.

### 2.2.4. *EDQNM run parameters*

A single calculation is considered at $Re_\lambda = 2500$ with the following parameters $k_0 = 1$, $v_0 = 1$ and $\nu = 10^{-5}$. The wavenumber mesh is chosen so that all the turbulent scales are well resolved. Mesh characteristics are hence set to $k_{\min} = 1/32$, $F = 8$ and $N = 165$.

Results are evaluated at $t^* = 8$ when self-similar decay of the kinetic energy spectrum occurs. This was ensured by checking that the eddy turnover time $q/\epsilon$ (where $\epsilon$ is the dissipation and $q = \int E(k)\,\mathrm{d}k$ is the total kinetic energy) increases as a power of law with time.

In order to improve the resolution of the results while calculating the nonlinear energy transfers at $t^* = 8$, the kinetic energy spectrum is linearly interpolated on a wavenumber mesh which is two times finer than the original mesh, with the following characteristics: $k_{\min} = 1/32$, $F = 16$ and $N = 328$.

### 2.3. *Filter transfer functions*

Discrete filters commonly used for LES are considered in this work. Filtering the variable $f$ on a uniform mesh can be performed using the central $(2N_f + 1)$-point algorithm, yielding

$$\overline{f}(x) = f(x) - \sum_{j=-N_f}^{N_f} d_j f(x + j\Delta), \tag{41}$$

where $d_j$ are the scheme coefficients and $\Delta$ is the mesh size. Taking the spatial Fourier transform of (41) provides the transfer function of the filter

$$G_k = \begin{cases} 1 - d_0 - \sum_{j=-N_f}^{N_f} 2d_j \cos(jk\Delta), & \text{if } k\Delta \leq \pi \\ 0, & \text{otherwise.} \end{cases} \tag{42}$$

The formal order of the filter represents the rate at which the transfer function converges to 1 when $k$ tends to zero. The coefficients of the standard filters are obtained thanks to a Taylor series by maximizing the formal order [4], which is then equal to $2N_f$. The transfer functions of the second- and tenth-order standard filters are presented in Figure 2 as an illustration. For both filters $G_k$ converges towards 1 as $k$ tends to zero. Compared to the low-order filter, the tenth-order filter exhibits a sharper slop so that the transition between the filtered and the unfiltered scales lies over a narrower wavenumber interval.

Note that the formal order of the filters can be reduced so that some coefficients are freely chosen. An optimization in the Fourier space can then be performed to design a filter with given spectral properties [3]. Such algorithms are widely used in the aeroacoustic community [21–23] because of their wide accuracy range.

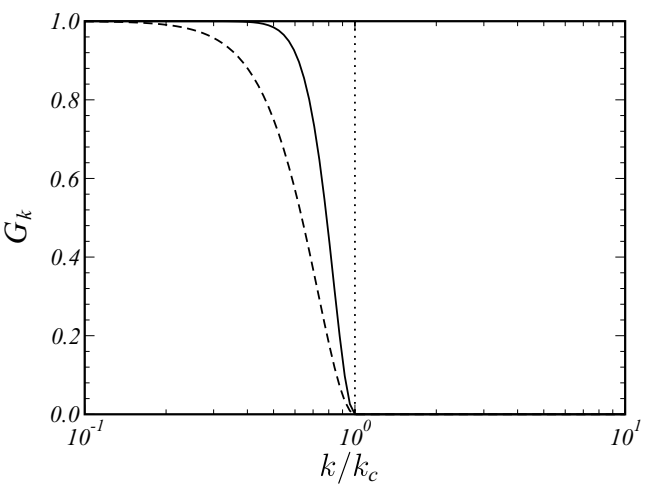


Figure 2. Transfer function of various filters as functions of the wavenumber $k/k_c$ normalized by the grid cut-off wavenumber $k_c$. – – –, second-order filter; ——, 10th-order filter; . . . . . ., spectral filter.

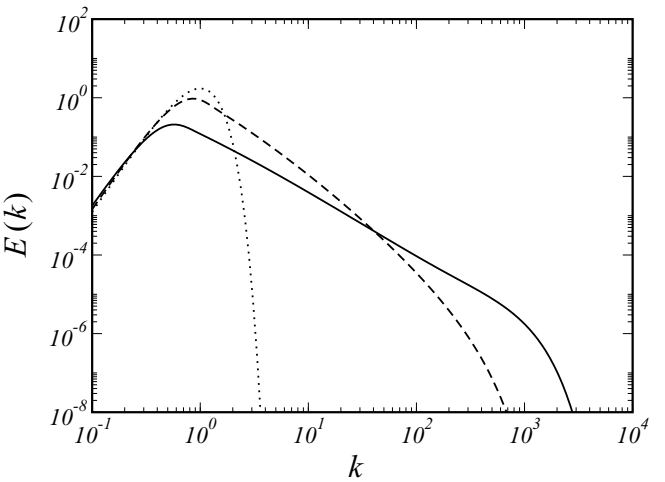


Figure 3. Time evolution of the kinetic energy spectrum $E(k)$ obtained by the EDQNM calculation ($Re_\lambda = 2500$). . . . . ., initial spectrum at $t^* = 0$; – – –, $t^* = 2$; ——, $t^* = 8$.

## 3. Results

### 3.1. *Evolved kinetic energy spectrum*

An overview of the time evolution of the EDQNM calculation in provided in Figure 3 where the kinetic energy spectrum is plotted for different time positions. The initial spectrum shows in particular a spectral content mainly clustered around the energy-containing scales at $k = k_0$. An intermediate spectrum obtained at $t^* = 2$ is also represented and exhibits a developing inertial range. As the computation is advanced in time, the initial spectrum converges towards a fully turbulent spectrum as the spectrum calculated for $t^* = 8$, which contains a maximum of energy in the neighbourhood of $k = k_0$ and an inertial range lying between $k = 1$ and $k = 10^3$. Above $k = 10^3$, a strong decrease of the kinetic energy is observed up to the Kolmogorov scale $k_\eta = 2\pi(\epsilon/\nu)^{1/4}$, which is around $k = 1.7 \times 10^4$ at $t^* = 8$.

### 3.2. *Scale separation*

The present EDQNM calculation is now used to quantify the nonlinear energy transfers defined in Section 2 for various filters. All the results presented in what follows are obtained with a grid cut-off wavenumber set to $k_c = 32$ and are evaluated at time $t^* = 8$.

As an illustration, the nonlinear energy transfers calculated for the fourth-order standard filter are first presented in Figure 4 as functions of the wavenumber $k/k_c$ normalized by the grid cut-off. The filtered nonlinear transfers $T^{\mathrm{nl}}(k)$, representing nonlinear interactions between filtered scales, exhibit a typical shape [24]. The negative values for $T^{\mathrm{nl}}(k)$ at large scales around $k/k_c = 1/32$ and the positive values at smaller scales, with $k/k_c > 10^{-1}$, correspond to the drain of energy from large to small scales due to the turbulence energy cascade. As expected, the non-represented and represented SGS energy transfers are negative since they aim at dissipating the energy produced at high wavenumbers by the triadic interactions.

Further details on the energy transfers are obtained by studying the normalized spectral eddy viscosities $\nu^+_{\mathrm{rep}}(k/k_c)$ associated with the represented energy transfers $T^{\mathrm{rep}}(k)$ corresponding to the couplings between the resolved scales $u_i^{\mathcal{L}}$. The spectral eddy viscosity $\nu^+_{\mathrm{nrp}}(k/k_c)$ is also

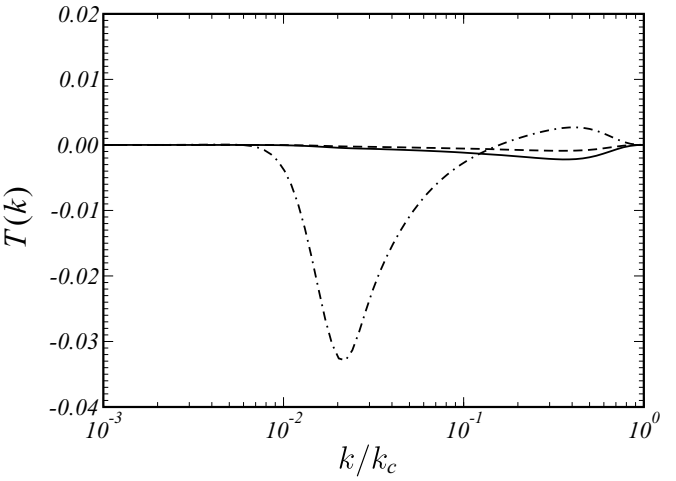


Figure 4. Snapshot of the nonlinear transfers at $t^* = 8$ for the fourth-order standard filter as functions of the wavenumber $k/k_c$ normalized by the grid cut-off. – · – · –, $T^{\mathrm{nl}}(k)$; – – –, $T^{\mathrm{nrp}}(k)$; ——, $T^{\mathrm{rep}}(k)$.

considered. It is deduced from the non-represented energy transfers $T^{\mathrm{nrp}}(k)$ due to the interactions involving the unresolved scales $u_i^S$. These two quantities are plotted in Figure 5 as functions of $k/k_c$ for the standard fourth-order filter under investigation. The non-represented SGS eddy viscosity $\nu^+_{\mathrm{nrp}}(k/k_c)$ shows a plateau for low wavenumbers corresponding to long-range triadic interactions between small scales sufficiently separated from the large scales [25]. Due to the filtering of the higher part of the spectrum, the classical cusp [19] close to the mesh cut-off is however no longer visible, and $\nu^+_{\mathrm{nrp}}(k/k_c)$ smoothly goes to zero when $k$ tends to $k_c$. Figure 5 demonstrates in addition that the non-represented and the represented SGS eddy viscosities have similar shapes for the present filter. One can also note that the amplitude of the represented

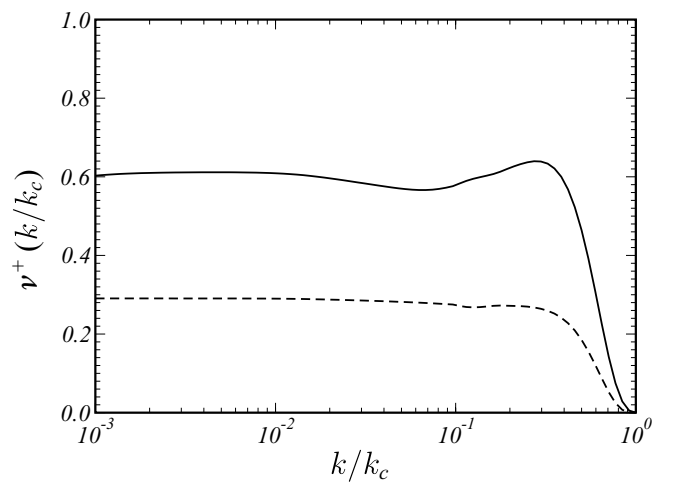


Figure 5. SGS nonlinear transfers at $t^* = 8$ for the fourth-order standard filter in terms of spectral eddy viscosity $\nu^+$ as functions of the normalized wavenumber $k/k_c$. ——, $\nu^+_{\mathrm{rep}}(k/k_c)$; – – –, $\nu^+_{\mathrm{nrp}}(k/k_c)$.

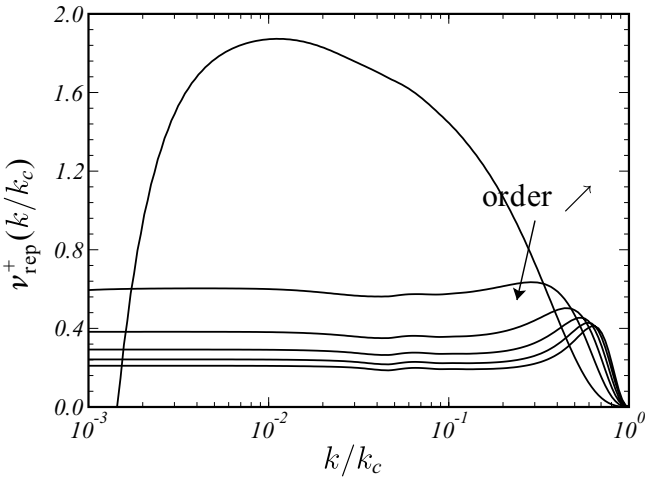


Figure 6. Represented scale spectral eddy viscosity $\nu^+_{\mathrm{rep}}(k/k_c)$ as functions of the normalized wavenumber $k/k_c$, at $t^* = 8$ and for $k_c = 32$. Results for standard filters of order from 2 to 12 are presented.

SGS transfers is significant since it is about two times larger than the non-represented SGS contributions.

Similar results are observed for most of the other standard filters. The represented SGS spectral eddy viscosity $\nu^+_{\mathrm{rep}}(k/k_c)$ is for instance plotted in Figure 6 for standard filters with order of accuracy ranging from 2 to 12. It turns out that with filters from 4th to 12th order, the represented SGS eddy viscosity displays the same typical shape: a plateau at large scales and a smooth decrease to zero close to the grid cut-off. A decrease of the spectral eddy viscosity is also visible as the formal order of the filter is higher, with plateau values around 0.6 for the fourth-order filter down to 0.3 for the 12th-order filter. The represented SGS tensor is indeed null for spectral filters because the spatial filtering and the spectral truncation are then identical implying that $\tau_{ij}^{\mathrm{rep}}$ given by Equation (4) is null. Taking a sharp cut-off transfer function therefore tends to nullify $\nu^+_{\mathrm{rep}}(k/k_c)$. Consider now the second-order filter. The represented SGS eddy viscosity does not exhibit a plateau for large scales, but rather a bump shape spanning a broad range of wavenumbers ($10^{-3} < k/k_c < 1$) and reaching high values with $\nu^+_{\mathrm{rep}}(10^{-2}) \simeq 1.8$ at its maximum. Thus, it seems that the second-order filter introduces a fundamentally different dynamics inside the represented SGS stress tensor $\tau_{ij}^{\mathrm{rep}}$.

A deeper investigation of the represented SGS tensor can be carried out by studying the contribution to the energy transfers scale-by-scale with the technique reported in Section 2.2.2. The focus is hence put on the detailed scale contribution

$$\zeta^{\mathrm{rep}}(k, k') = \frac{\partial}{\partial k'}\left[\iint_{\Delta^<_{k|k'}} \gamma^{\mathrm{rep}}_{kpq} S(k, p, q)\,\mathrm{d}p\mathrm{d}q\right] \tag{43}$$

of the represented SGS energy transfers $T^{\mathrm{rep}}(k)$. This quantity is represented in Figure 7 for $k = 1$ as a function of $k'/k_c$ for the standard filters with order from 2 to 12. For filters from 4th to 12th order, the detailed contributions are similar: they are close to zero for low wavenumbers and show negative values in the vicinity of the grid cut-off wavenumber. This demonstrates that for these filters the represented SGS energy transfers at $k = 1$ are dominated by interactions between scales belonging to the higher part of the energy spectrum. Non-zero values of the detailed

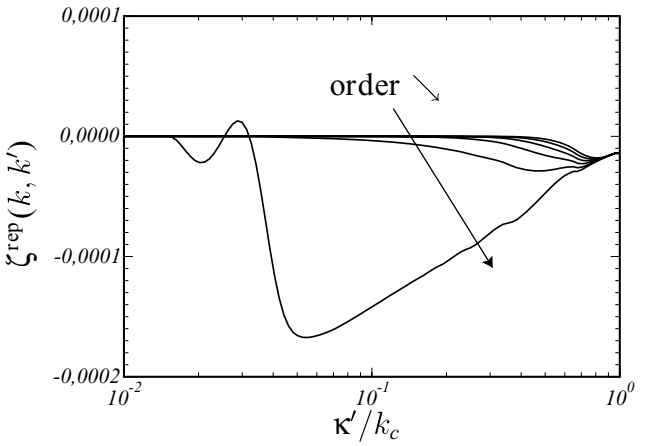


Figure 7. Detailed scale contribution $\zeta^{\text{rep}}(k, k')$ to the represented nonlinear energy transfers for a reference wavenumber $k = 1$ as a function of $k'/k_c$, at $t^* = 8$ and for $k_c = 32$. Results for standard filters of order from 2 to 12 are presented.

contribution $\zeta^{\text{rep}}(k, k')$ are furthermore seen to be more and more clustered around the grid cut-off wavenumber as the order of the filter is increased. Concerning the second filter, the detailed contribution to the represented SGS energy transfers $T^{\text{rep}}(k)$ exhibits in Figure 7 non-negligible values over a large range of wavenumbers $3 \times 10^{-3} < k'/k_c < 1$ and reaches a negative minimum for $k'/k_c = 5 \times 10^{-3}$ in the neighbourhood of the energy-containing scales. The represented SGS energy transfers $T^{\text{rep}}(k)$ at $k = 1$ is thus dominated by large-scale interactions for the second-order filter.

Detailed contributions can be more precisely investigated in Figure 8(a) which presents $|\zeta^{\text{rep}}(k, k')|$ for $k = 1$ in logarithmic scales as a function of $k'$. Note that the modulus of $\zeta^{\text{rep}}$ is taken since it is mainly negative. The influence of the filter order is clearly observed with a progressive decrease of the contribution of low wavenumbers when the order is increased. For sharper cut-off filter, the detailed contribution $\zeta^{\text{rep}}(k, k')$ is indeed seen to be more clustered around the grid cut-off wavenumber and a steeper convergence to zero is observed when $k'$ tends towards large scales. Figure 8(b) presents $\zeta^{\text{rep}}(k, k')$ for a reference wavenumber $k = 4$, corresponding to $k/k_c = 0.125$, in logarithmic scales as a function of $k'$. It turns out that the trends are identical to those obtained for the case $k = 1$. Increasing the filter order makes small-scale interactions dominate the represented SGS energy transfers $T^{\text{rep}}(k)$. The second-order filter is also found to lead to represented SGS energy transfers mainly driven by large scales since $\zeta^{\text{rep}}(k, k')$ is maximum for $k/k_c \simeq 0.15$ for instance in Figure 8(b).

The formal order of the filter is thus directly related to the physical interpretation of the represented SGS stress tensor $\tau_{ij}^{\text{rep}}$. For the second-order filter, the present results demonstrate that the tensor $\tau_{ij}^{\text{rep}}$ is dominated by large-scale dynamics. This point breaks the very basis of LES which rely on the assumed universal behaviour of small-scale interactions contributing to the SGS stress tensor. Stefano and Vasilyev [6] already mentioned this trend during their study of the filtered Burger's equation. The second-order filter therefore does not seem to be an adequate choice. Increasing the order of accuracy nevertheless permits to make the represented SGS stress tensor be dominated by interactions between scales lying in the upper part of the energy spectrum, so that the universality hypothesis of the SGS stress tensor is fulfilled.

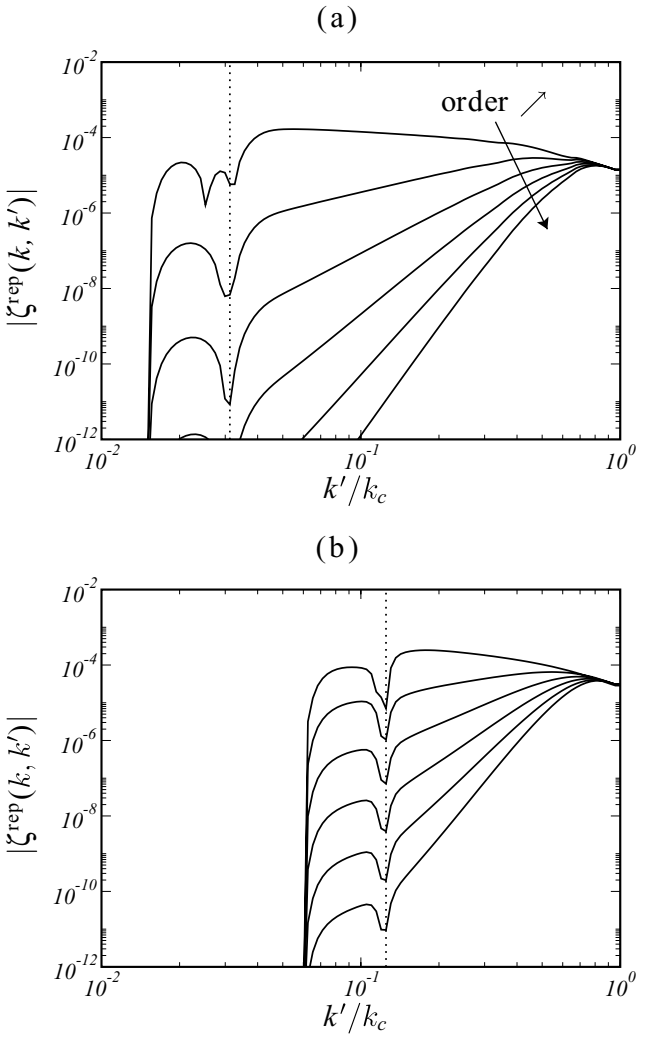


Figure 8. Detailed scale contribution $|\zeta^{\mathrm{rep}}(k, k')|$ to the represented nonlinear energy transfers for two reference wavenumbers $k$ as a function of $k'/k_c$, at $t^* = 8$ and for $k_c = 32$, in logarithmic scales. Standard filters of order from 2 to 12 are presented. (a) $k = 1$; (b) $k = 4$. The dotted line indicates where the reference wavenumber is located on the axis $k'/k_c$.

### 3.3. *Effective LES cut-off wavenumber*

Scale separation hence appears strongly dependent on the filter shape, an attempt is now conducted to quantify at which scale the spectrum is split into two parts by the filter.

Scale separation is illustrated by Figure 9(a) where the detailed scale contribution $|\zeta^{\mathrm{SGS}}(k, k')|$ is plotted for the total SGS energy transfers $T^{\mathrm{SGS}}(k) = T^{\mathrm{rep}}(k) + T^{\mathrm{nrp}}(k)$ as a function of $k'$, at $k = 1$ and for the standard filters of order 4–12. The detailed scale contribution is seen to be split into two parts. Above the grid cut-off wavenumber, for $k'/k_c > 1$, it is filter independent and contributes to the non-represented SGS energy transfers $T^{\mathrm{nrp}}(k)$ involving unresolved scales $u_i^S$. For $k' < k_c$ it is dependent on the filter shape, and contributes to the represented SGS energy transfers $T^{\mathrm{rep}}(k)$ due to the resolved scales $u_i^{\mathcal{L}}$. Note that the left-side part of the curves is identical to the plots of Figure 8(a). Therefore, as pointed out in the

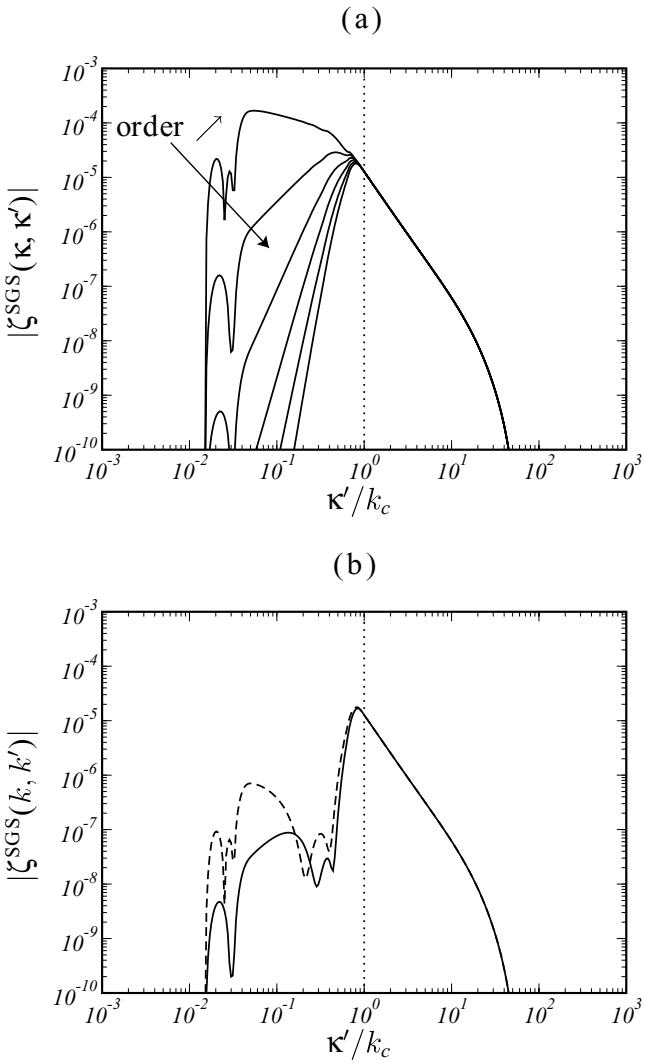


Figure 9. Detailed scale contribution $|\zeta^{SGS}(k, k')|$ to the classical SGS energy transfers for a reference wavenumber $k = 1$ as a function of $k'/k_c$, at $t^* = 8$ and for $k_c = 32$, in logarithmic scales. (a) Standard filters of order from 4 to 12 and (b) optimized filters of Bogey and Bailly [3]: – – –, 11-point filter; ——, 13-point filter.

former section, one can observe that a wide range of scales, including resolved ones, participates to the SGS stress tensor. High-order filters nevertheless lead to a sharp cut-off at high wavenumbers.

Increasing the order of the filtering is hence an efficient technique to allow a better use of the mesh spectral support. For sufficiently large stencil filters, the formal order can also be reduced, and the filter transfer function can be optimized in the Fourier space [3]. Figure 9(b) presents for instance the detailed scale contribution $|\zeta^{SGS}(k, k')|$ for the total SGS stress tensor as a function of $k'$, at $k = 1$ and for the 11-point second-order and the 13-point fourth-order filters of Bogey and Bailly [3]. Below the grid cut-off wavenumber, for $k' < k_c$, a sharp cut-off is visible on the

detailed contributions for both optimized filters. This cut-off is steeper than the cut-off observed for the 12th-order standard filter in Figure 9(a).

Evaluating the effective LES cut-off wavenumber requires to elaborate a criterion defining which scales participate or not to the SGS stress tensor. Based on Figure 9(a), this can be done by introducing an arbitrary criterion on the contribution amplitude. The present work makes use of the following criterion: $k_s$ is determined as the smallest wavenumber such as $|\zeta^{\mathrm{SGS}}(k, k_s)| > 10^{-6}$. The effective LES cut-off is then defined as $k_s/k_c$ which tends to 1 for sharp cut-off filters. The quantity $\zeta^{\mathrm{SGS}}(k, k_s)$ however depends on the reference wavenumber $k$ so that the cases $k = 1$, $k = 2$ and $k = 4$ are studied here to check whether the proposed definition of the effective LES cut-off is robust or not.

The effective LES cut-off wavenumber $k_s/k_c$ is plotted in Figure 10(a) as a function of the number of points of the algorithm, for the standard and optimized filters and for reference wavenumbers $k$ equal to 1, 2 and 4. The curves obtained for the three values of $k$ show little dispersion and demonstrate that the proposed definition for $k_s/k_c$ is robust. As already pointed out in Section 3.2, increasing the order of the filter makes the effective LES cut-off wavenumber larger, with, for $k = 1$ for instance, values ranging from $k_s/k_c = 0.05$ for the second-order filter and up to $k_s/k_c = 0.4$ for the 12th-order scheme. The ratio between these two extrema is about 8. In term of point-per-wavelength, the 10th and 12th filters lead to a scale separation at about 5 points per wavelength. Concerning the two optimized filters, they exhibit the largest effective LES cut-off wavenumbers with $k_s/k_c$ equal to 0.45 and 0.5 for the 11-point and 13-point schemes, respectively. These limits correspond to approximately 4 point-per-wavelength waves. It is worth noting that optimization of the filters was precisely performed in order to yield filters with a cut-off lying at 4 point-per-wavelength waves [3].

The efficiency of the filters in terms of computational cost is furthermore a matter of interest. The efficiency rate $e_s$ of a discrete filter is defined in this work as the inverse of the total number of operations that would be required to perform a scale separation at $k_c$ instead of $k_s$. The number of operations is first proportional to the number of points $2N_f + 1$ of the algorithm. Then, to shift the scale separation $k_s$ towards $k_c$, the mesh size must be divided by $k_c/k_s$ so that the number of points is multiplied by $(k_c/k_s)^3$ for a three-dimensional grid. The efficiency rate of a discrete filter is therefore defined here as

$$e_s = \frac{1}{(2N_f + 1)\,(k_c/k_s)^3}. \tag{44}$$

The efficiency rates of the standard and optimized filters are shown in Figure 10(b) as a function of the number of points of the algorithm for reference wavenumbers $k$ equal to 1, 2 and 4. Note that the efficiency rates are normalized by the value obtained for the 13-point optimized filter of Bogey and Bailly [3]. The results indicate that increasing the filter order widens the spectral resolution in an efficient manner since the efficiency rate increases monotonically with the formal order: from 0.0001 for the second-order filter to about 0.5 for 12th-order one. The efficiency rates also show that the optimization of the filters leads to a relevant gain since the rates of the optimized filters are about two times larger than those obtained with the standard filters using the same number of points.

Finally, the influence of the criterion used to evaluate the effective LES cut-off wavenumber is investigated for the standard schemes. The results previously reported are based on the assumption that the LES cut-off wavenumber $k_s$ is the smallest wavenumber $k'$ such as $|\zeta^{\mathrm{SGS}}(k, k')| > A$, with a threshold $A = 10^{-6}$. One may nevertheless choose another values for $A$. The effective cut-off wavenumbers $k_s/k_c$ are then plotted in Figure 11(a) for the standard filters using the thresholds $A = 10^{-8}$, $A = 10^{-7}$, $A = 10^{-6}$ and $A = 10^{-5}$. The efficiency rates of the standard

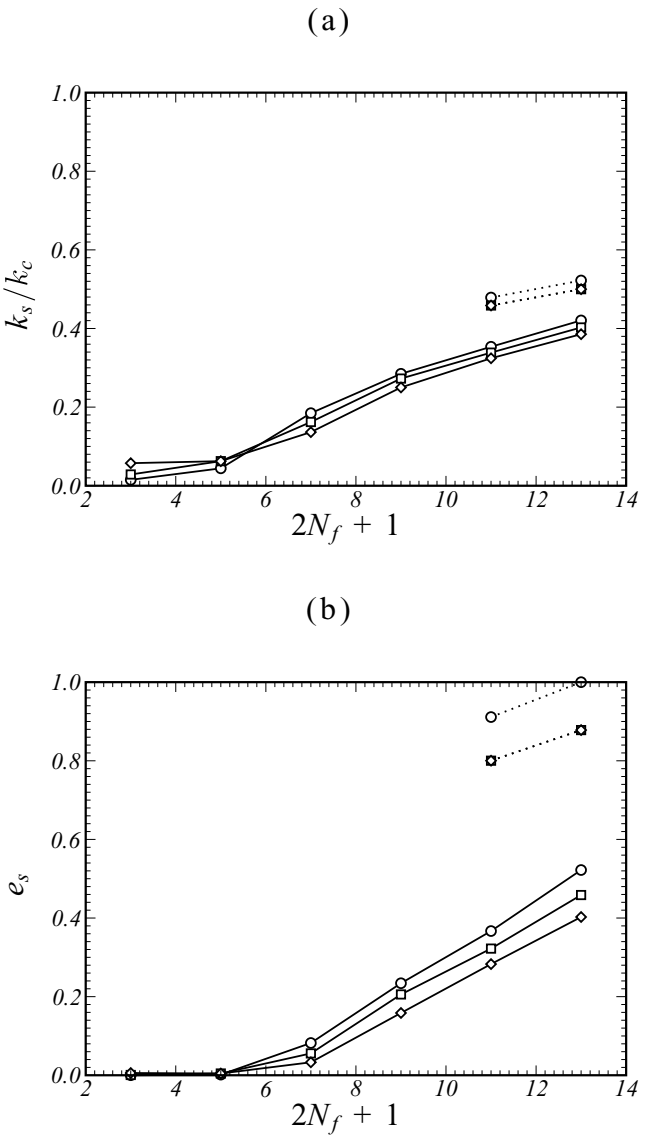


Figure 10. (a) Effective LES cut-off $k_s/k_c$ and (b) efficiency rates $e_s$ for the standard and optimized filters as function of the number of points $2N_f + 1$ of the algorithm. ——, standard filters; . . . . . ., optimized filters. Reference wavenumber: ○, $k = 1$; □, $k = 2$; ◇, $k = 4$.

filters are also represented in Figure 11(b) for these values of $A$. As expected, the LES cut-off wavenumbers differs with the value of the threshold $A$. The main trend is nonetheless the same and is consistent with previous conclusions: the effective cut-off wavenumber increases with the order of the scheme. The efficiency rates in Figure 11(b) further support this point because high-order algorithms exhibit the higher efficient rates for the four values of the threshold $A$. The case $A = 10^{-5}$ however exhibits some discrepancies. The 11-point discrete filter is for instance observed to be more efficient than the 13-point algorithm. Nevertheless, the detailed scale contribution $|\zeta^{\mathrm{SGS}}(k, k')|$ of the total SGS stress tensor reaches a maximum of about

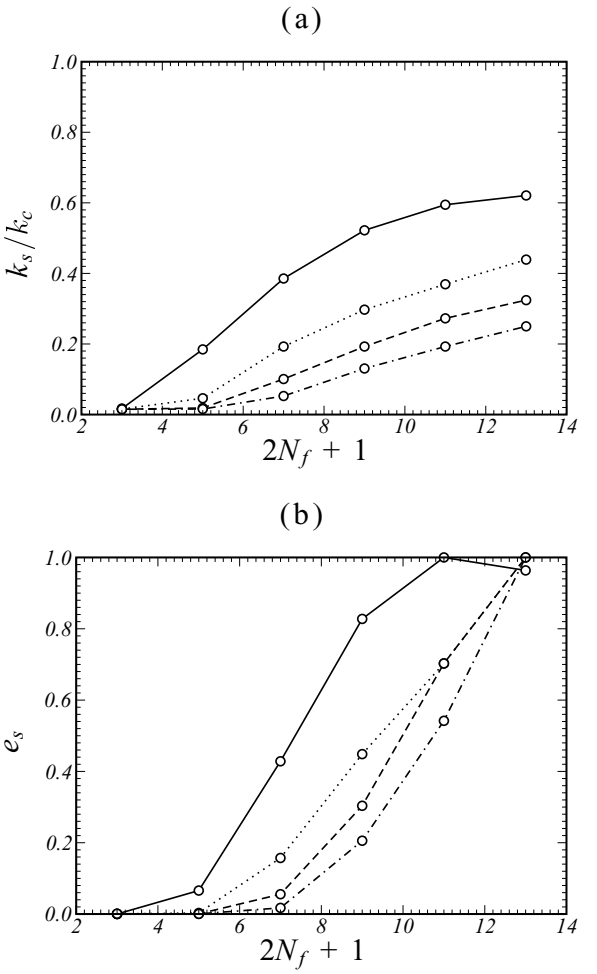


Figure 11. (a) Effective LES cut-off $k_s/k_c$ and (b) efficiency rates $e_s$ for the standard filters as a function of the number of points $2N_f + 1$ of the algorithm, and for several scale separation criteria: ——, $A = 10^{-5}$; . . . . . , $A = 10^{-6}$; – – –, $A = 10^{-7}$; – · – · –, $A = 10^{-8}$. The reference wavenumber is $k = 1$.

$2 \times 10^{-5}$ for the 11- and 13-point schemes. Taking $A$ equal to $10^{-5}$ is thus a rather high value for the threshold, and the scale separation criterion may loose its relevancy.

## 4. Conclusion

Following Domaradzki and Adams [5], explicit reference to the spectral truncation associated with the projection of the velocity field on a grid has been used to derive the filtered incompressible Navier–Stokes equations. The classical SGS stress tensor has been decomposed into a so-called represented SGS tensor representing nonlinear interactions between scales present on the grid, and into a non-represented SGS tensor taking into account interactions involving non-resolved scales.

An EDQNM model for the filtered incompressible Navier–Stokes has been proposed to evaluate the represented and non-represented stress tensor for standard and optimized discrete

filters for a Reynolds number $Re_\lambda = 2500$. In order to determine which scales contribute mostly to the SGS tensors, a procedure allowing us to compute contributions scale-by-scale to nonlinear energy transfers has been elaborated. The technique has been applied to the non-represented stress tensor. For the second-order standard filter, it turned out that the non-represented stress tensor is dominated by large-scale interactions. The universality assumption of the SGS stress tensor hence cannot be fulfilled. This is fortunately not the case using filters with order greater than four, for which the non-represented stress tensor is mainly driven by interactions between scales close to the mesh cut-off. Based on these observations, the effective LES cut-off wavenumber has been evaluated for the standard filters and for two optimized filters. The spectral resolution is found to widen with the order of the filter as well as with the optimization of the transfer function. The effective cut-off wavenumber has been recast in terms of efficiency rates to take into account the computational effort to achieve a given spectral resolution. The results reveal that the efficiency rate increases with the order of the filter. In addition, the optimized filters, which exhibit the higher efficiency rates, seem to be well appropriate to achieve sharp and efficient scale separation in LES.

Considering this, using spectral filters for practical large-eddy simulations appears to be the most suitable filtering technique. Discussions on the interpretation of the SGS tensor or on the effective cut-off wavenumbers are then circumvented. When spectral operators cannot be designed for the flow configuration studied, discrete filters, with smooth transfer functions, are to be implemented. The filter shape must then be sharp enough to ensure that the SGS stress tensor is dominated by small-scale dynamics. In addition, the computational cost and the effective LES cut-off wavenumber need to be balanced.

**Acknowledgements**

The authors would like to thank W. Bos for helpful discussions about the EDQNM modelling approach.

**References**

[1] B. Geurts, *Elements of Direct and Large-Eddy Simulation*, Edwards, Philadelphia, PA, 2003.
[2] C. Fureby and G. Tabor, *Mathematical and physical constraints on large-eddy simulations*, Theor. Comput. Fluid Dyn. 9 (1997), pp. 85–102.
[3] C. Bogey and C. Bailly, *A family of low dispersive and low dissipative explicit schemes for flow and noise computations*, J. Comput. Phys. 194 (2004), pp. 194–214.
[4] O.V. Vasilyev, T.S. Lund, and P. Moin, *A general class of commutative filters for LES in complex geometry*, J. Comput. Phys. 146 (1998), pp. 82–104.
[5] J.A. Domaradzki and N.A. Adams, *Direct modelling of subgrid scales of turbulence in large eddy simulations*, J. Turbul. 3 (2002), pp. 1–19.
[6] G.D. De Stefano and O.V. Vasilyev, *Sharp cutoff versus smooth filtering in large eddy simulation*, Phys. Fluids 14 (2002), pp. 362–369.
[7] S. Pope, *Ten questions concerning the large-eddy simulation of turbulent flows*, New J. Phys. 6 (2004), pp. 1–24.
[8] C. Bogey and C. Bailly, *Large eddy simulations of transitional round jets: Influence of the Reynolds number on flow development and energy dissipation*, Phys. Fluids 18 (2006), #065101.
[9] D. Carati, G.S. Winckelmans, and H. Jeanmart, *On the modelling of the subgrid-scale and filtered-scale stress tensors in large-eddy simulation*, J. Fluid Mech. 441 (2001), pp. 119–138.
[10] J.A. Langford and R.D. Moser, *Optimal LES formulations for isotropic turbulence*, J. Fluid Mech. 398 (1999), pp. 321–346.
[11] J.A. Domaradzki and K.C. Loh, *The subgrid-scale estimation model in the physical space representation*, Phys. Fluids 11 (1999), pp. 2330–2342.
[12] ———, *Large eddy simulations using the subgrid-scale estimation model and truncated Navier–Stokes dynamics*, Theor. Comput. Fluid Dyn. 15 (2002), pp. 421–450.

[13] U. Piomelli, P. Moin, and J. Ferziger, *Model consistency in large eddy simulation of turbulent channel flows*, Phys. Fluids 31 (1988), pp. 1884–1891.
[14] D. Leslie and G. Quarini, *The application of turbulence theory to the formulation of subgrid modelling procedures*, J. Fluid Mech. 91 (1979), pp. 65–91.
[15] X. Yang and S. Fu, *The effect of filtering on truncated Navier-Stokes equations*, J. Turbul. 8 (2007), pp. 1–18.
[16] J.A. Domaradzki and D. Carati, *A comparison of spectral sharp and smooth filters in the analysis of nonlinear interactions and energy transfer in turbulence*, Phys. Fluids 19 (2007), #085111.
[17] O. Schilling and Y. Zhou, *Analysis of spectral eddy viscosity and backscatter in incompressible, isotropic turbulence using statistical closure theory*, Phys. Fluids 14 (2002), pp. 1244–1258.
[18] M. Lesieur, *Turbulence in Fluids*, Kluwer, Dordrecht, 1987.
[19] J.-P. Chollet and M. Lesieur, *Parametrization of small scales of three-dimensional isotropic turbulence utilizing spectral closures*, J. Atmos. Sci. 38 (1981), pp. 2747–2757.
[20] C. Leith, *Atmospheric predictability and two-dimensional turbulence*, J. Atmos. Sci. 28 (1971), pp. 145–161.
[21] C. Tam, *Computational aeroacoustics: Issues and methods*, AIAA J. 33 (1995), pp. 1788–1797.
[22] S.K. Lele, *Compact finite difference schemes with spectral-like resolution*, J. Comput. Phys. 103 (1992), pp. 16–42.
[23] M.R. Visbal and D.V. Gaitonde, *Very high-order spatially implicit schemes for computational acoustics on curvilinear meshes*, J. Comput. Acoust. 9 (2001), pp. 1259–1286.
[24] S. Pope, *Turbulent Flows*, Cambridge University Press, Cambridge, 2000.
[25] R. Kraichnan, *Eddy viscosity in two and three dimensions*, J. Atmos. Sci. 33 (1976), pp. 1521–1536.
[26] S. Orszag, *Analytical theories of turbulence*, J. Fluid Mech. 41 (1970), pp. 363–386.
[27] J. Bertoglio, F. Bataille, and J. Marion, *Two-point closures for weakly compressible turbulence*, Phys. Fluids 13 (2001), pp. 290–310.
[28] C. Cambon and L. Jacquin, *Spectral approach to non-isotropic turbulence subjected to rotation*, J. Fluid Mech. 202 (2002), pp. 295–317.

## Appendix. The EDQNM modelling

The EDQNM (eddy-damped quasi-normal Markovian) theory, which has been first formalized by Orszag [26], is a spectral stochastic closure applied to homogeneous isotropic incompressible turbulence. Some of the hypotheses can be relaxed, as for instance in [27] and [28], but more evolved models are not needed for the present study. The EDQNM method aims at determining the time evolution of the kinetic energy spectrum $E(k, t)$. Starting from the Navier–Stokes equations in spectral space, schematically written as

$$\left(\frac{\partial}{\partial t} + \nu k^2\right) u = uu, \tag{45}$$

one can show that the governing equations of the double- and triple-velocity correlations are given by

$$\left(\frac{\partial}{\partial t} + 2\nu k^2\right) \langle uu \rangle = \langle uuu \rangle, \tag{46}$$

$$\left[\frac{\partial}{\partial t} + \nu(k^2 + p^2 + q^2)\right] \langle uuu \rangle = \langle uuuu \rangle, \tag{47}$$

where $\langle \cdot \rangle$ is an ensemble average. The kinetic energy spectrum $E(k, t)$ is directly related to the double-velocity correlations $\langle uu \rangle$. Resolution of Equation (46) is hence of special interest but as shown in (47), the triple correlations $\langle uuu \rangle$ on the right-hand side of (46) are unclosed terms which need to be modelled.

The quasi-normal hypothesis is first introduced. The velocity field is assumed to be close to a Gaussian state and the fourth-order moments $\langle uuuu \rangle$ can then be expressed in terms of the double-velocity correlations with $\langle uuuu \rangle = \sum \langle uu \rangle \langle uu \rangle$. Eddy damping is necessary to ensure the realizability of the

kinetic energy spectrum. Based on these assumptions, Equation (47) now reads as,

$$\left[\frac{\partial}{\partial t} + \nu(k^2 + p^2 + q^2)\right]\langle uuu\rangle = \sum\langle uu\rangle\langle uu\rangle - (\mu_k + \mu_p + \mu_q)\langle uuu\rangle, \tag{48}$$

where $\mu_k$ is the eddy-damping rate for a wavenumber $k$. Integration of the above equation with respect to time variable $t$ yields,

$$\langle uuu\rangle(t) = \int_0^t \sum\langle uu\rangle\langle uu\rangle \mathrm{e}^{-\Omega_{kpq}t}\,\mathrm{d}t, \tag{49}$$

with $\Omega_{kpq} = \mu_k + \mu_p + \mu_q + \nu k^2 + \nu p^2 + \nu q^2$. Further simplification can be achieved by assuming that the time scale of the second-order moments $\langle uu\rangle$ is large compared to that of the eddy-damping (the Markovian process). The equation for the triple-velocity correlations finally reads as

$$\langle uuu\rangle(t) = \Theta(t)\sum\langle uu\rangle\langle uu\rangle, \tag{50}$$

where $\Theta(t) = \int_o^t \mathrm{e}^{-\Omega_{kpq}t}\,\mathrm{d}t$ is a relaxation time. Introducing closure (50) into the governing Equation (46) of the double-velocity correlations $\langle uu\rangle$ finally permits to calculate the time evolution of the kinetic energy spectrum $E(k, t)$.

In the framework of the present study, the explicit formulation (50) for the triple-velocity correlations can be directly introduced into the right-hand side of the governing Equation (17) for the kinetic energy $\overline{E}(k, t)$ of the filtered velocity field.